

**Distribution Agreement**

In presenting this thesis as a partial fulfillment of the requirements for a degree from Emory University, I hereby grant to Emory University and its agents the non-exclusive license to archive, make accessible, and display my thesis in whole or in part in all forms of media, now or hereafter now, including display on the World Wide Web. I understand that I may select some access restrictions as part of the online submission of this thesis. I retain all ownership rights to the copyright of the thesis. I also retain the right to use in future works (such as articles or books) all or part of this thesis.

Shoeb Lallani

March 23, 2017

Neuropathology of Striatal Interneurons in Transgenic Nonhuman  
Primate Models of Huntington's Disease

By

Shoeb Lallani

Dr. Anthony W.S. Chan, DVM, PhD  
Adviser

Department of Neuroscience and Behavioral Biology

Anthony W.S. Chan, DVM, PhD  
Adviser

Yoland Smith, PhD  
Committee Member

Matthew Weinschenk, PhD  
Committee Member

Rosa M. Villalba, PhD  
Committee Member

In Ki Cho, PhD  
Committee Member

2017

Neuropathology of Striatal Interneurons in Transgenic Nonhuman  
Primate Models of Huntington's Disease

By

Shoeb Lallani

Dr. Anthony W.S. Chan, DVM, PhD  
Adviser

An abstract of  
a thesis submitted to the Faculty of Emory College of Arts and Sciences  
of Emory University in partial fulfillment  
of the requirements of the degree of  
Bachelor of Sciences with Honors

Department of Neuroscience and Behavioral Biology

2017

## Abstract

### Neuropathology of Striatal Interneurons in Transgenic Nonhuman Primate Models of Huntington's Disease

By Shoeb Lallani

Huntington's disease (HD) is an autosomal dominant neurodegenerative disorder characterized by chorea, dystonia, ataxia, cognitive impairment, and psychiatric disturbances. The genetic cause of HD is an expansion of a cysteine-adenine-guanine (CAG) trinucleotide repeat in exon one of the human huntingtin (*HTT*) gene, which leads to a poly-glutamine (poly-Q) expansion in the huntingtin (HTT) protein. The poly-Q expansion results in production and accumulation of polyglutamine aggregates and leads to regional-specific brain atrophy in the striatum and cortex. This atrophy is due mainly to the loss of striatal projection neurons, while interneurons are relatively spared. To better understand the progressive mechanism of HD and the development of therapeutic agents against HD, an animal model that can recapitulate human conditions including neuropathology and progressive clinical manifestation is important to advance our knowledge about HD. Because of close physiological, neurological, and genetic similarities between humans and nonhuman primates (NHPs), monkeys can serve as valuable models for understanding the underlying mechanism of HD. Our lab has developed a transgenic NHP model of human HD that exhibits progressive clinical manifestation similar to human HD patients. In this project, we performed in-depth stereological analysis on wild-type (WT) and HD-NHPs to evaluate the total number and density of calretinin (CR), parvalbumin (PV), and choline acetyltransferase (ChAT)-positive striatal interneurons. Our results show striatal atrophy and tendency of interneurons to be spared, which is consistent with studies in HD patients. We also see differences in the two HD-NHPs that are reminiscent of juvenile and adult progressions

of HD. This study provides further support of our HD-NHP model and its potential to serve as a preclinical animal model of HD.

Neuropathology of Striatal Interneurons in Transgenic Nonhuman  
Primate Models of Huntington's Disease

By

Shoeb Lallani

Dr. Anthony W.S. Chan, DVM, PhD

Adviser

A thesis submitted to the Faculty of Emory College of Arts and Sciences  
of Emory University in partial fulfillment  
of the requirements of the degree of  
Bachelor of Sciences with Honors

Department of Neuroscience and Behavioral Biology

2017

## Acknowledgements

I would first and foremost like to thank Dr. Anthony W.S. Chan, Dr. Yolanda Smith, Dr. Matthew Weinschenk, Dr. Rosa M. Villalba, and Dr. In Ki Cho for being a part of senior honors thesis committee and for their taking the time to assist me with my project.

I want to thank Dr. Chan and Dr. Smith for their constant guidance and support throughout my project. I would like to thank Dr. Rosa M. Villalba for her assistance with the stereology, and constant guidance throughout the project. I would like to thank Dr. In Ki Cho for his educational support and guidance with qPCR and logistics. I would like to thank Ms. Susan Jenkins for her assistance with tissue processing and immunohistochemical staining of the brain sections. I would also like to thank Ms. Amy Wang for her support with qPCR.

I would like to thank the SIRE and SURE programs for providing funds to support my project. I would like to also thank the Transgenic Huntington's Disease Monkey Resource sponsored by the Office of Research Infrastructure Programs (ORIP) - OD010930 – and the NIH, Office of Research Infrastructure Programs (ORIP/OD) - P51-OD011132 – for their support of this project and the Yerkes National Primate Research Center.

I would like to thank Yerkes National Primate Center and its staff for their support with the care of the animals. I would also like to thank the rest of my colleagues in the Chan and Smith labs for their continuous support throughout the project.

## Table of Contents

<b>Abstract .....</b>	<b>1</b>
<b>Background .....</b>	<b>2</b>
Huntington's disease.....	2
Striatal Cell Loss in HD.....	5
In Vitro Models of HD.....	6
Animal Models of HD .....	7
Preliminary Work.....	9
<b>Objectives .....</b>	<b>11</b>
<b>Introduction to Stereology.....</b>	<b>12</b>
<b>Material and Methods.....</b>	<b>14</b>
Ethics Statement.....	14
Animal models.....	14
Tissue preparation .....	14
Immunohistochemistry .....	15
Stereology .....	16
<b>Results .....</b>	<b>17</b>
<b>Stereology .....</b>	<b>17</b>
Calretinin (CR) .....	17
Parvalbumin (PV).....	18
Choline Acetyltransferase (ChAT) .....	19

<b>Discussion .....</b>	<b>21</b>
<b>Differences Between rHD1 and rHD7 .....</b>	<b>21</b>
<b>Comparisons with HD Patients .....</b>	<b>22</b>
<b>Why Are These Interneurons Relatively Spared? .....</b>	<b>23</b>
<b>Conclusions .....</b>	<b>25</b>
<b>Future Directions.....</b>	<b>26</b>
<b>Figures .....</b>	<b>27</b>
<b>Figure 1. Stereology .....</b>	<b>27</b>
<b>Figure 2. Pre- and Post-Commissural Regions.....</b>	<b>28</b>
<b>Table 1. Number of Sections and Serial Section Interval Number .....</b>	<b>29</b>
<b>Table 2. Optical Fractionator Grid and Counting Probe Size .....</b>	<b>30</b>
<b>Table 3. Interneuron Counts and Percent Difference .....</b>	<b>31</b>
<b>Table 4. Striatal Volume and Percent Difference .....</b>	<b>32</b>
<b>Table 5. Interneuron Density and Percent Difference .....</b>	<b>33</b>
<b>Figure 3. Stereological Counts of CR+ Neurons .....</b>	<b>34</b>
<b>Figure 4. Stereological Counts of PV+ Neurons .....</b>	<b>35</b>
<b>Figure 5. Stereological Counts of ChAT+ Neurons .....</b>	<b>36</b>
<b>Figure 6. Light Micrographs of Immunostained Striatal Interneurons.....</b>	<b>37</b>
<b>References .....</b>	<b>38</b>

## Abstract

Huntington's disease (HD) is an autosomal dominant neurodegenerative disorder characterized by chorea, dystonia, ataxia, cognitive impairment, and psychiatric disturbances. The genetic cause of HD is an expansion of a cysteine-adenine-guanine (CAG) trinucleotide repeat in exon one of the human huntingtin (*HTT*) gene, which leads to a poly-glutamine (poly-Q) expansion in the huntingtin (HTT) protein. The poly-Q expansion results in production and accumulation of polyglutamine aggregates and leads to regional-specific brain atrophy in the striatum and cortex. This atrophy is due mainly to the loss of striatal projection neurons, while interneurons are relatively spared. To better understand the progressive mechanism of HD and the development of therapeutic agents against HD, an animal model that can recapitulate human conditions including neuropathology and progressive clinical manifestation is important to advance our knowledge about HD. Because of close physiological, neurological, and genetic similarities between humans and nonhuman primates (NHPs), monkeys can serve as valuable models for understanding the underlying mechanism of HD. Our lab has developed a transgenic NHP model of human HD that exhibits progressive clinical manifestation similar to human HD patients. In this project, we performed in-depth stereological analysis on wild-type (WT) and HD-NHPs to evaluate the total number and density of calretinin (CR), parvalbumin (PV), and choline acetyltransferase (ChAT)-positive striatal interneurons. Our results show striatal atrophy and tendency of interneurons to be spared, which is consistent with studies in HD patients. We also see differences in the two HD-NHPs that are reminiscent of juvenile and adult progressions of HD. This study provides further support of our HD-NHP model and its potential to serve as a preclinical animal model of HD.

## Background

### *Huntington's disease*

Huntington's disease (HD) is an autosomal dominant neurodegenerative disorder that affects hundreds of thousands of people around the world. The disease is more commonly seen in majority-Caucasian countries including Europe, Australia, and North America (Pringsheim et al., 2012). On average, HD affects 3-10 per 100,000 adults in Western Europe and North America, and juvenile cases account for 4.92% of these HD cases (Gil and Rego, 2008; Quarrell et al., 2012). HD onset is between the ages of one and 80, and clinical features include chorea, dystonia, memory loss, ataxia, and psychiatric disturbances. These symptoms are highly related to polyglutamine (poly-Q) size (Walker, 2007). Children suffering from the juvenile form of HD develop symptoms that differ from the adult form, including bradykinesia, while chorea may be absent (Rubinsztein, 2002). Presentation of these symptoms is useful in HD diagnosis, but can often be misdiagnosed as other neurological disorders. HD can be accurately diagnosed by genetic testing based on the size of the CAG tract in the huntingtin (*HTT*) gene. Patients with HD are usually given medication to alleviate emotional and motor instability, but there currently is no way to treat or reverse the course of the disorder. The disease usually results in death 10 to 15 years after the onset of symptoms (Walker, 2007).

HD is characterized by the expansion of a trinucleotide sequence in the *HTT* gene. The *HTT* gene is located on the short arm of chromosome four (O'Donovan, 1993; Gil and Rego, 2008). The function of the WT-*HTT* is still elusive, but some data suggests its importance in post-implantation development and the normal functioning of the basal ganglia. *HTT* knockout in mice is embryonically lethal (Nasir et al., 1995). Huntingtin is also involved in the regulation of

transcription and transportation of brain-derived neurotrophic factor (BDNF) (Zuccato et al., 2001).

Within the *HTT* gene, there is a repeated cysteine-adenine-guanine (CAG) sequence located at the 5' terminus that codes for the amino acid glutamine (Q). Normal individuals have 35 or fewer CAG repeats (35Q), and repeat numbers greater than 40Q is considered to be the mutant *HTT* (*mHTT*) variant. Incomplete penetrance occurs when there are 36-40Q (Rubinsztein et al., 1996; Penney et al., 1997). In general, the greater the number of repeats, the earlier the onset and increased severity of HD (O'Donovan, 1993). Adult HD typically occurs with an inheritance of a poly-Q size around 40-55 repeats, and onset is usually between 35 and 55 years of age (Rubinsztein et al., 1996). Patients with adult onset show slower progression of the disease, suffering from chorea that may evolve into dystonia. Juvenile HD occurs with an inheritance of a poly-Q that exceeds 60 repeats. Early onset HD tends to progress more rapidly and can culminate to more severe clinical features (Illarioshkin et al., 1994; Quarrell et al., 2013).

The major theory of molecular pathogenesis of HD is that the expansion of the CAG repeats confers a gain-of-function effect via the overproduction of glutamine at the N-terminus. These polyglutamines will begin to aggregate by forming dimers, trimer, and oligomers, resulting in neuronal intranuclear inclusion bodies (DiFiglia et al., 1997; Schulte and Littleton, 2011). These nuclear aggregates are suspected to be the major culprit of the neurodegeneration seen in HD patients, although no conclusive mechanism has been determined (Walker, 2007; Ross and Tabrizi, 2011). Other studies have shown dysregulation of the production of BDNF, as well (Zuccato et al., 2001). *In vivo* studies have demonstrated that HD causes an upregulation of a polyglutamine-expanded form of the HPRT protein. Mice with increased levels of this protein

developed a late-onset neurological phenotype that progressed to premature death (Ordway et al., 1997).

Although the exact mechanism for HD has yet to be elucidated, evidence supports that HD preferentially targets the striatum and the cortex initially (Walker, 2007; Ross and Tabrizi, 2011). The striatum is part of the basal ganglia, which is situated at the base of the forebrain. The principle components of the basal ganglia are the striatum, the pallidum, the substantia nigra, and the subthalamic nucleus. It is believed that the basal ganglia work in a parallel processing manner by which they receive cortical inputs, which are then processed and distributed to other cortical regions. The basal ganglia regulate a wide variety of functions ranging from emotional regulation to procedural learning. Most importantly, basal ganglia are vital in the basal ganglia-thalamocortical circuitry, which functions to regulate voluntary movement. In normal conditions, the cortex and substantia nigra pars compacta would stimulate the striatum to initiate voluntary movement. The striatum then sends signals down two separate pathways: a direct pathway and an indirect pathway. The direct pathway is believed to stimulate the desired movement to occur, while the indirect pathway inhibits antagonistic movements (Smith et al., 1998; Calabresi et al., 2014). This combination allows for smooth, directed muscle contractions and visually-guided movements (Cui et al., 2013). In HD patients, there is atrophy of striatal projection neurons along both the direct and indirect pathways, although studies in animal models have shown that neurons of the indirect pathway degenerate earlier (Cepeda et al., 2007; Andre et al., 2011). This results in dysfunction in the basal ganglia-thalamocortical tract, accounting for some of the hyperkinesia seen in HD patients (Parent et al., 1995; Centonze et al., 2007).

### *Striatal Cell Loss in HD*

Aside from glial cells, projection neurons make up the vast majority of cells in the striatum. These projection neurons connect the striatum to the rest of the basal ganglia regions that are involved in the motor, associative, and limbic circuitry. Post-mortem studies in HD patients have shown that there is a selective loss of projection neurons that interconnect the striatum to globus pallidus and substantia nigra (Centonze et al., 2007). The depletion of these projection neurons accounts for the striatal atrophy in HD patients. Studies have also demonstrated the progressive nature of HD, with juvenile HD patients suffering from greater loss of projection neurons and more severe atrophy of the striatum as compared to adult onset patients (Reiner et al., 1988).

Unlike projection neurons, striatal interneurons modulate communication amongst neurons within the same brain region. Interneurons of the striatum are subcategorized based on their neurochemical content: calretinin (CR), parvalbumin (PV), choline acetyltransferase (ChAT), and  $\beta$ -nicotinamide adenine dinucleotide phosphate-diaphorase (NADPH-d). CR and PV are calcium-binding proteins, ChAT is an enzyme involved in the synthesis of acetylcholine, and NADPH-d is nitric oxide synthase (Cicchetti et al., 2000). CR-expressing (CR+) interneurons constitute the vast majority of interneurons in the human striatum (Cicchetti et al., 1998). CR+ interneurons can be further classified as large (22-29  $\mu\text{m}$ ), multipolar neurons with 5-7 aspiny, highly branched dendrites, or as medium (9-13  $\mu\text{m}$ ), round-to-oval neurons with 2-3 varicose, poorly branched dendrites (Parent et al., 1995). Post-mortem neuropathological analysis of HD patients have shown that there is selective loss of large CR+ interneurons, but not of medium-sized CR+ interneurons (Cicchetti et al., 1998). Medium CR+ interneurons often do not co-express any of the other three markers of striatal neurons. However, large CR+

interneurons also often display ChAT immunoreactivity as well. Decreased striatal density of these large interneurons are found in HD patients, suggesting a possible underlying factor in the selective neurodegeneration (Cicchetti et al., 1998; Massouh et al., 2008). Little is known about the other markers of striatal neurons, but, in general, interneurons are seen to be relatively spared compared to projection neurons in HD (Cicchetti et al., 1996).

### *In Vitro Models of HD*

To better understand the pathological, cellular, and molecular mechanisms of HD, model systems that recapitulate human HD conditions are necessary. *In vitro* models have been useful in investigating striatal neural cell functions influenced by *mHTT*. The reprogramming of HD patients' somatic cells into induced pluripotent stem cells (iPSCs) is pivotal in understanding the cellular and molecular pathogenesis of HD and the development of novel therapeutic strategies for HD patients (Juopperi et al., 2012). iPSCs that carry identical mutations to patients can be differentiated into various neural cell types, such as GABA and TH neurons, providing a unique platform for investigating the effect of *mHTT* on specific neuronal cell functions (Carter et al., 2014). iPSCs are also considered a prominent cell source in cell replacement therapy, which has shown great promise in animal models (Juopperi et al., 2012).

Although there are practical uses for this *in vitro* model of HD, there are limitations. First, the microenvironment which the differentiated iPSCs are placed into does not entirely resemble that of the human brain. There are differences in exposure of these cells to modifiers including growth factors and intercellular interactions. Due to these differences, neuronal cells derived via iPSCs have been shown to lack some phenotypic characteristics seen in patients' cells (Juopperi et al., 2012). Also, differentiating naïve cells to one cell line is difficult, and

multiple cell lines are often present. Therefore, achieving a homogenous population of the desired cell line is challenging (Fong et al., 2010).

### *Animal Models of HD*

Animal models are important for understanding the disease progression and pathogenesis, as well as for evaluating therapeutic efficacy of novel treatments. Although it is challenging to create an animal model that recapitulates all the molecular, pathological, and behavioral features of a disease, many animal models can effectively recreate some aspects of the disorder. Mice are a common choice for modeling human diseases. Among HD mice models, R2/6 mice are the most commonly used in HD research. The R2/6 mice begin to show motor deficits, including tremors and abnormal gait, as early as five weeks of age. However, lack of striatal atrophy was observed in R6/2 mice as compared to HD patients (Davies et al., 1997; Morton et al., 2000). The N171-82Q mouse model shows intranuclear inclusions that are immunoreactive with an antibody to the N-terminus of HTT, as seen in HD patients. Both these rodent models recapitulate some behavioral phenotypes, including loss of coordination and abnormal gait, and some neuroanatomical changes of HD. There are many other rodent models of HD, as well, that effectively reflect aspects of human HD (Menalled and Chesselet, 2002).

Although rodent models have been useful in recapitulating behavioral phenotypes of HD, the animal model is constrained in two respects: first, the short lifespan of rodents makes it difficult to perform longitudinal studies of HD in this model. HD is a progressive disorder that takes many years to develop in humans and the short lifespan of a rodent model does not allow for investigation of the progressive nature of the disease (Morton and Howland, 2013). Second, the rodent brain differs from the human brain both in size and neuroanatomy. In particular, the

two regions of interest in HD, the striatum and cortex, vary widely between rodents and humans. The mouse striatum does not contain separate nuclei for the caudate and putamen, and the cortex of mice is significantly smaller than in humans (Treuting et al., 2012). Differences in striatal interneuron populations of mice and humans have also been noted. The most abundant striatal interneuron found in mice is PV+, while in humans, CR+ interneurons make up the vast majority of interneuronal cells. In addition, a nonuniform distribution of CR+, PV+, and NADPH-d+ interneurons was observed in mice, with higher densities of all these interneurons in the rostral striatum than in the caudal regions. In contrast, these striatal interneurons are uniformly distributed throughout the human striatum (Wu and Parent, 2000). Also, in mice, there is little to no presence of medium-sized interneurons co-expressing CR and ChAT, while these interneurons are commonly seen in humans (Petryszyn et al., 2014).

Unlike mice, nonhuman primates (NHPs) are very similar to humans, both in their genomic makeup and neuroanatomy (Herculano-Houzel, 2009). NHPs share similar interneuron characteristics and patterns with humans. The primary difference between NHPs and humans is that NHPs have a higher density of total striatal interneurons than humans (Wu and Parent, 2000). NHPs have also presented with motor dysfunction upon lesion of the basal ganglia (Ferrante et al., 1993; Storey et al., 1994; Burns et al., 1995; Kendall et al., 2000). Finally, the lifespan of NHPs is longer than rodents, allowing for better progressive analysis of HD. These data indicate that NHPs have the potential to serve as progressive and neuroanatomical models of HD.

### *Preliminary Work*

Given the neuroanatomical similarities between monkeys and humans, NHPs have the potential to serve as a valuable model for HD. We have developed the first transgenic NHP model of HD (HD-NHP) with progressive decline in cognition and behavioral impairment. Rhesus macaques (*Macaca mulatta*) carry 1-10 poly-Q repeats in the *HTT* gene, while humans normally carry 9-35 repeats (Putkhao et al., 2013). The HD-NHPs were generated by transfecting mature oocytes using a high titer lentivirus vector expressing exon 1 with 29Q of the human *HTT* gene regulated by the human ubiquitin promoter C (rHD1) or expressing exons 1-10 with ~70Q of the human *HTT* gene regulated by the human *HTT* promoter (rHD7). The presence of the transgenes in the HD-NHPs was confirmed by polymerase chain reaction (PCR) analysis, and expression of the transgenic *mHTT* was confirmed by quantitative PCR (qPCR) and Western blot analysis (Yang et al., 2008).

HD-NHPs developed a gradual decline in motor functions and visuomotor performance when compared to control NHPs, similar to symptoms observed in human HD patients (Feigin et al., 1995). As the disease progressed, volume reduction in caudate nucleus and putamen were determined by longitudinal MRI. Significant enlargement of the ventricles in rHD1 was noted. Immunohistochemistry on post-mortem brain sections showed the presence of aggregates and nuclear inclusion bodies in the striatum of the HD-NHPs, while expression levels of *mHTT* was also revealed in corresponding areas with higher amounts of aggregation. The barrier test was conducted on the HD-NHPs, and rHD7 showed motor decline indicative of striatal dysfunction. Although longitudinal MRI did not show significant changes in the striatal volume of rHD7, striatal atrophy was demonstrated through stereological analysis of the Nissl-positive cells (Chan et al., 2014; Chan et al., 2015). These results bear a strong resemblance to behavioral and

anatomical changes observed in human HD patients, suggesting that our NHP model may recapitulate some behavioral and neuroanatomical changes associated with HD.

## Objectives

The purpose of this study was to further validate our HD-NHP model. HD patients develop striatal atrophy due to a loss of projection neurons in the caudate nucleus and putamen, with a relative sparing of the interneurons in the region (Reiner et al., 1988; Cicchetti et al., 1996; Halliday et al., 1998). These interneurons express unique protein markers after which they are named: calretinin (CR), parvalbumin (PV),  $\beta$ -nicotinamide adenine dinucleotide phosphate-diaphorase (NADPH-d), and choline acetyltransferase (ChAT) (Cicchetti et al., 2000).

Prior studies in HD-NHPs show similar clinical features including psychomotor symptoms that resemble those seen in HD patients (Chan et al., 2014; Chan et al., 2015). To better understand the underlying neuropathological mechanism of HD in HD-NHPs, we propose an examination of the changes in the number and density of three major subtypes of striatal interneuron: CR+, PV+, and ChAT+.

We conducted a stereological comparison between two HD-NHPs and one WT-NHP by examining three striatal interneuron subpopulations. Stereology allows for an unbiased estimation of the total number of each interneuron subtype, and the Cavalieri's principle allows us to estimate the volume of the striatum. Using these data sets, we will calculate the density of each interneuron subpopulation in the striatum. We will also differentiate between the rostral and caudal regions of the striatum in attempt to assess potential differences in the extent of HD-induced degeneration between the different striatal functional regions, as previously shown in HD patients (Vonsattel et al., 1985; Rub et al., 2016). We will compare the data between the two HD-NHPs and the WT-NHP, as well as with the data from HD patients.

## Introduction to Stereology

In the current study, we continue our efforts to validate the efficacy of our transgenic HD-NHP model by conducting a stereological analysis of control and transgenic HD-NHP brain sections. Stereology is a subset of morphometry, which is used to obtain data on three-dimensional structures from two-dimensional planar surfaces (Altunkaynak et al., 2012). This technique is useful for studying brain regions because it allows investigators to perform unbiased counting of the number of cells expressing a specific marker within the region of interest (ROI). To utilize this method, the brain of interest is typically flash-frozen and sliced into thin sections. The sections that contain the ROI are then identified and images were serially captured. Of this entire brain ROI, a subset of representative sections are selected in a serial fashion (e.g. one every twelve slices, one every fifteen slices). The serial sections are then immunostained for the marker of interest and mounted onto slides.

The stereology software, Stereo Investigator (mbf Bioscience), is utilized to count the number of positively marked cells in the ROI of each serial section. The thickness of the brain slices, the interval number for the serial sections, and the total number of sections are entered. For each slide, the ROI is delineated and dimensions for an optical fractionator grid and counting probe are determined. The optical fractionator grid is overlaid on the ROI in a random fashion, and every time the grid is reset, the grid will be adjusted so that different areas of the ROI fall within different boxes of the grid. Each box of the grid contains a smaller box which is the counting probe. The investigator only counts the number of positively marked cells that fall within the boundaries of the probe. Each probe has two acceptance (green) lines and two rejections (red) lines to fairly account for marked cells that fall on the outer boundaries of the probe (Figure 1). The Stereo Investigator then navigates the investigator through each of the

probes, and the investigator marks each positively stained cell that is identified. This same method is repeated for each slide in the set, using the same dimensions for the optical fractionator grid and counting probe. Upon completion of all the sections, Stereo Investigator presents an estimated total cell count for the entire ROI along with a coefficient of error (CE) value (West, 2012).

The CE value is a quantified number that provides information on how precise the total cell count estimate is. The CE number is determined by the total number of marks the investigator places during the counting of cells within the probes. The greater the number of markers placed, the more precise the total estimate is (lower CE) (Glaser and Wilson, 1998). However, a minimum of 250 markers must be placed for the program to process the information accurately. The number of markers placed is dependent on the number of positively stained cells seen in the counting probes. Therefore, one can decrease the CE by increasing the size of the probe (increase the area where cells are counted), decreasing the size of the grid (increase the number of grid squares, and therefore the number of counting probes), or increasing the number of sections that are counted (decrease the serial interval number). However, the CE can be handicapped if the total number of cells of interest is known to be low. In this case, regardless of how many sections are counted or how many probes are designed, the total number of markers may not be high enough to lower the CE (Glaser and Wilson, 1998).

## Material and Methods

### *Ethics Statement*

All procedures were performed at the Yerkes National Primate Research Center (YNPRC) and were approved by the Emory University Institutional Animal Care and Use Committee (IACUC). All procedures were approved by the Emory Health and Biosafety Committee (EHSO).

### *Animal models*

For stereological analysis, three NHPs were used. rHD1 was a five-year-old male transgenic HD-NHP who was generated via lentiviral transfer of exon 1 of the mutant *HTT* transgene with 29Q repeats regulated by human ubiquitin-C promoter and a green fluorescent protein (GFP) regulated by human ubiquitin-C promoter for visualization. rHD7 was a five-year-old male transgenic HD-NHP who was generated via a lentiviral transfer of exons 1-10 of the mutant *HTT* gene with 70Q repeats regulated by a human *HTT* promoter. Both HD-NHPs were euthanized due to the development of HD phenotypes and self-injury behavior which is not uncommon in nursery-raised captive NHPs. rWT1 was a four year old male NHP who served as the control.

### *Tissue preparation*

NHPs were deeply anesthetized via pentobarbital overdose (100 mg/kg) at the time of euthanasia. rWT1 was perfused with a mixture of paraformaldehyde (4% PFA) and glutaraldehyde (0.1%). For the brains of the HD-NHPs, one hemisphere was post-fixed in 4% PFA, saturated in 30% sucrose, serially sectioned and cryopreserved. The contralateral

hemisphere was dissected into constituent regions, cut into smaller pieces, snap frozen in liquid nitrogen, and stored in  $-80^{\circ}\text{C}$ . After fixation, the brains were washed with PBS to remove the paraformaldehyde, saturated in 30% sucrose, serial frozen-sectioned into  $50\ \mu\text{m}$  thick coronal slices and stored in an anti-freeze solution (1.4%  $\text{NaH}_2\text{PO}_4\text{-H}_2\text{O}$ , 2.6%  $\text{Na}_2\text{HPO}_4$ , 30% ethylene glycol, 30% glycerol in  $\text{H}_2\text{O}$ ) in  $-20^{\circ}\text{C}$ .

### *Immunohistochemistry*

Brain slices from the NHPs that contained the striatum were collected. To test for possible regional difference in the extent of degeneration, we separated the serial sections into the rostral and caudal striatum, using the anterior commissure as the landmark between the pre-commissural and post-commissural striatal regions (Figure 2).

Serial sections from the one control (rWT1) and two transgenic HD-NHPs (rHD1, rHD7) were organized: for PV and CR staining, 1 in every 24 sections were used for rHD1 and rHD7 and 1 in every 15 sections were used for rWT1; for ChAT staining, 1 in every 24 sections were used for rWT1 and 1 in every 12 sections were used for rHD1 and rHD7 (Table 1). These sections were stained using a mouse primary antibody: mouse anti-CR (1:1,000, SWAT catalog #6B3), mouse anti-PV (1:10,000, SWAT catalog #235), goat anti-ChAT (1:100, Prosci catalog #50-265). The sections were incubated in blocking buffer overnight at room temperature, washed with PBS several times, and then incubated with the associated biotinylated secondary antibody (1:200; Vector Laboratories) for 90 minutes. Avidin-biotin-peroxidase complex (ABC kit, Vector) in PBS/Tris buffer (50 mM; pH7.6) was applied to the sections and diaminobenzidine (DAB, Sigma) was used as a chromogen for the peroxidase reaction to reveal the positive

staining. Sections were then rinsed with PBS, mounted onto gelatin-coated slides, and covered by coverslips.

### *Stereology*

Using the computer software Stereo Investigator (mbf Bioscience) and the Optical Fractionator probe (optical dissector technique), we individually estimated the total number of CR+, PV+, or ChAT+ interneurons in the caudate nucleus and putamen of the control and transgenic HD-NHPs. The delineation of the ROI was performed at low magnification (2.5x), while the counts of the neurons (profiles) were conducted with a 40x oil-immersion objective (Figure 1). The ROI was divided and sampled in a superimposed virtual grid to maximize efficiency and minimize the CE (Table 2).

The Cavalieri's principle (grid of points: 400x400 $\mu$ m) was then utilized to estimate the volumes of the caudate nucleus and putamen in each NHP. The delineation of the caudate nucleus and putamen and the unbiased volume estimation were performed under low magnification (2.5x) by multiplying the sum of the caudate nucleus and putamen areas by the distance between the sections (Altunkaynak et al. 2012). The precision of the estimates of the total number of neurons was evaluated by the CE, which is determined based on the dimensions of the probe and the total number of positively marked cells counted in the ROI for each animal (Glaser et al. 1998).

## Results

### *Stereology*

For this study, we utilized serial sections from two HD-NHPs (rHD1 and rHD7) and one WT-NHP (rWT1) to estimate the number of CR+, PV+, and ChAT+ interneurons in the caudate nucleus and putamen (Table 1, Table 2). We also used Cavalieri's principle to estimate the total striatal volume in each NHP. We then extrapolated interneuronal density by using the counts and striatal volume.

### Calretinin (CR)

Immunostained CR+ cells were counted in the striatum of the three NHPs. Stereological analysis revealed that rHD1 had about 16% of CR+ neurons in the caudate head compared to rWT1, and rHD7 had 10% more CR+ neurons in the caudate head compared to the control. In the caudate body, both HD-NHPs had fewer CR+ cells compared to rWT1, with rHD1 and rHD7 showing 42% and 22% fewer neurons, respectively (Figure 3A). In the putamen, a similar trend was seen. rHD1 and rHD7 had near similar numbers of CR+ cells in the pre-commissural putamen, while in the post-commissural putamen, rHD1 and rHD7 had 44% and 28% fewer CR+ cells than control, respectively. (Figure 3B, Table 3).

Volume measurements showed that rHD1 had a 60% smaller caudate nucleus than rWT1. rHD7 showed a 33% larger caudate head and a 15% smaller caudate body compared to control (Figure 3C). The putamen showed a similar result; rHD1 had a 53% smaller pre-commissural putamen and a 73% smaller post-commissural putamen. rHD7 had a 12% larger pre-commissural putamen and a 20% smaller post-commissural putamen than control (Figure 3D, Table 4).

Density calculations portrayed a 110% higher density in the caudate head and a 58% higher density of CR+ cells in the caudate body of rHD1 compared to control. rHD7 showed a 17% and 9% lower density of CR+ cells in the caudate head and body, respectively, compared to rWT1 (Figure 3E). Analysis of the putamen yielded similar results, with rHD1 showing a 113% and 107% higher CR+ cell density than control in the pre-commissural and post-commissural putamen, respectively. In contrast, rHD7 showed 3% and 9% lower CR+ densities in the pre- and post-commissural regions, respectively (Figure 3F, Table 5).

### Parvalbumin (PV)

Stereological analysis of PV+ cells in the striatum of the three NHPS was also conducted. Both transgenic HD-NHPs had fewer PV+ neurons in the caudate nucleus compared to control. rHD1 had 56% and 75% fewer PV+ cells in the caudate head and body, respectively. The caudate head of rHD7 contained 47% fewer PV+ neurons, and the caudate body contained 80% fewer PV+ cells than control (Figure 4A). The transgenic HD-NHPs also showed fewer PV+ neurons in the putamen compared to rWT1. rHD1 had 8% fewer PV+ cells in the pre-commissural putamen, and 39% fewer in the post-commissural putamen. rHD7 contained 32% and 64% fewer PV+ cells in the pre- and post-commissural putamen, respectively (Figure 4B, Table 3).

Investigation of the striatal volume in these sets of serial sections revealed a similar trend to the one seen above. In rHD1, the caudate head and body was 52% and 62% smaller than in rWT1 (Figure 4C), while the volume of the pre- and post-commissural putamen was reduced by 57% and 77%, respectively, compared to rWT1. (Figure 4D). rHD7 had similar volumes for the

rostral regions of the striatum, but had a 27% and 35% smaller caudate body and post-commissural putamen, respectively, compared to control (Figure 4C, Figure 4D, Table 4).

Density analysis showed that rHD1 had 9% and 35% lower PV+ density in the caudate head and body, but had 113% and 162% greater PV+ cell density in the pre- and post-commissural putamen, compared to rWT1 (Figure 4E, Figure 4F). rHD7 showed a nearly 50% lower PV+ cell density in the caudate head, and a 72% lower density in the caudate body (Figure 4E). In the putamen, rHD7 had a 34% lower PV+ density pre-commissurally, and a 44% lower PV+ density post-commissurally (Figure 4F, Table 5).

#### Choline Acetyltransferase (ChAT)

The number of ChAT+ cells in the striatum of the three NHPs were analyzed. rHD1 had 27% more ChAT+ cells in the caudate head, and 12% fewer in the caudate body, relative to rWT1. rHD7 had 11% more ChAT+ cells in the caudate head, and 56% fewer ChAT cells in the caudate body (Figure 5A). In the putamen, rHD1 contained 25% and 50% fewer ChAT+ neurons pre- and post-commissurally, while rHD7 contained 48% and 88% fewer ChAT+ neurons pre- and post-commissurally (Figure 5B, Table 3).

Analysis of striatal volume showed that rHD1 had a 51% and 62% smaller rostral and caudal caudate nucleus relative to rWT1 (Figure 5C). The putamen of this NHP was 61% smaller in the pre-commissural region and 71% smaller in the post-commissural region (Figure 5D). rHD7 had 35% and 19% larger pre-commissural caudate nucleus and putamen, relative to control, but had a 39% and 18% smaller post-commissural caudate nucleus and putamen, respectively (Figure 5C, Figure 5D, Table 4).

Interneuronal density showed a substantially higher density of the interneuron in rHD1, which had 157% and 129% greater ChAT+ cell density in the caudate head and body than did the control (Figure 5E). The putamen of rHD1 also had higher ChAT+ densities, being 94% higher in the pre-commissural putamen and 79% higher in the post-commissural putamen (Figure 5F). rHD7, however, showed lower ChAT+ cell density throughout the striatum, compared to rWT1. The ChAT+ cell density of rHD7 was 17% and 28% lower in the caudate head and body, and 56% and 86% lower in the pre- and post-commissural putamen, respectively (Figure 5E, Figure 5F, Table 5).

## Discussion

This study was conducted to further investigate the neuropathology of HD-NHP model to better understand the mechanism of the disease progression, which will help develop and test new treatment for HD in HD-NHPs. Our transgenic HD-NHP model has shown behavioral and psychomotor symptoms seen in HD patients (Chan et al., 2014; Chan et al., 2015; Raper et al., 2016). This stereological investigation was undertaken to investigate the changes in the neuronal makeup of the striatum. Studies show that HD patients suffer from striatal atrophy because of a loss of projection neurons, which make up a majority of the striatum (Reiner et al., 1988). Striatal interneurons, on the other hand, seem to be relatively spared (Cicchetti et al., 1996). We examined our transgenic HD-NHPs to see if they recapitulate this aspect of HD striatal pathology.

Three of the main interneurons found in the human striatum display calretinin (CR), parvalbumin (PV), or choline acetyltransferase (ChAT) immunoreactivity (Cicchetti et al., 2000). We immunostained brain slices of the transgenic HD-NHPs and a control NHP for each of these markers, and performed unbiased cell counts via stereology. The rostral and caudal regions of the striatum were considered as separate ROI in our counting in an attempt to assess possible regional differences in the extent of striatal interneuron pathology seen in HD monkeys. We used Cavalieri's principle to measure changes in striatal volume between the transgenic HD-NHPs and the WT-NHP. Densities of the striatal interneurons were also calculated.

### *Differences Between rHD1 and rHD7*

Our data show some differences in interneuron numbers between the two HD-NHPs. This variance is most likely due to the difference in the nature of the two *mHTT* transgenes. rHD1

carried exon 1 of the human *HTT* gene regulated by the human polyubiquitin-C promoter with 29Q, while rHD7 carried exons 1-10 of the human *HTT* gene with 70Q repeats, and was regulated by the human *HTT* promoter. Due to the wide expression of the *mHTT* transgene regulated by the human polyubiquitin-C promoter and exon 1 of the *HTT* gene, rHD1 was expected to develop more aggressively, as shown through behavioral assessments, suggesting that rHD1 is reminiscent of the juvenile form of HD. rHD7, on the other hand, carried a larger *HTT* fragment which was regulated by human *HTT* promoter, and was expected to resemble endogenous *HTT* expression patterns and slower progression of HD, as shown in our longitudinal studies ((Chan et al., 2014; Chan et al., 2015). Thus, the changes in striatal pathology in the two HD monkeys might represent the progressive development in mild and manifested HD monkeys (Illarioshkin et al., 1994; Rubinsztein et al., 1996; Chan et al., 2015).

The data from our stereological analysis support our hypothesis that the two HD-NHPs present progressive HD neuropathology. More severe striatal atrophy in rHD1 was observed when compared to rHD7. We also saw greater deviations in striatal interneuron count and density from control for rHD1 than for rHD7. Since the two transgenic HD-NHPs were the same age at the time of euthanasia, the severity of the striatal pathology was more advanced in rHD1 than in rHD7. This is consistent with prior reports on the clinical and molecular assessments of the two monkeys with distinct HD development trajectory and their resemblance to juvenile and adult forms of HD (Chan et al., 2015).

### *Comparisons with HD Patients*

Our results provide further evidence for a dramatic decrease in the striatal volume of rHD1 compared to the control (Chan et al., 2014). It also reemphasizes the fact that rHD7 also

showed reduction in striatal volume as well, it does not seem to be as severe as was in rHD1 (Chan et al., 2015). Both HD-NHPs suffer a more severe striatal shrinkage in the caudal regions of the striatum, which suggests that the caudal region of the striatum is preferentially affected prior to the rostral striatum. This is supported by the difference in total interneuron counts between the transgenic HD-NHPs and the WT-NHP. Interneuron counts in the caudal regions of the striatum of the transgenic HD-NHPs differed the most from the control. Thus, consistent with human findings, these data suggest that striatal pathology of HD originates in the caudal striatum and expands rostrally as it progresses (Vonsattel et al., 1985; Rub et al., 2016).

The decreased striatal volume seen in HD patients has been attributed to atrophy caused by the death of striatal projection neurons, while interneurons remain relatively spared (Cicchetti et al., 1996; Cicchetti and Parent, 1996). We saw a similar trend in our transgenic HD-NHPs; although the total number of interneurons is decreasing, the density of those interneurons was strikingly higher in the transgenic HD-NHPs compared to the control NHP (Figure 6). This could mean that, although interneurons are lost, other cells of the striatum, such as projection neurons, must be degenerating at a faster rate than these interneurons. This would explain the simultaneous decrease in interneuron count and increase in interneuron density along with the loss of striatal mass. The increased density of striatal interneurons is consistent with HD patient data (Cicchetti et al., 1996; Cicchetti and Parent, 1996; Cicchetti et al., 1998; Massouh et al., 2008).

### *Why Are These Interneurons Relatively Spared?*

Although interneurons survive longer than projection neurons in HD patients, the mechanism involving this protection remains unknown. There are two possibilities as to how this

might occur: these proteins (CR and PV) are neuroprotective and allow interneurons to better elude degeneration or striatal cells are upregulating gene expression for these neuroprotective proteins to better elude degeneration. Both of these hypotheses center around the idea that these proteins may provide protection against neurodegeneration. One popular hypothesis for the mechanism of neurodegeneration in HD is that neuronal degeneration is elicited by the disruption of calcium homeostasis in neurons. This dysregulation can result in the toxic accumulation of calcium in the cell cytoplasm and lead to neurodegeneration (Luthi-Carter et al., 2000; Hansson et al., 2001; Zucker et al., 2005). Thus, high expression of calcium-binding proteins, including CR and PV in interneurons, could better buffer abnormal elevations of intracellular calcium concentrations and maintain calcium homeostasis.

## Conclusions

Our results show that the transgenic HD-NHPs have decrease striatal volume, especially in the caudal regions of the striatum. The transgenic HD-NHPs also show a decrease in the number of interneurons in the striatum, but an increase in the interneuron density, especially in the caudal regions of the caudate nucleus and putamen. These HD-NHPs display pathological features of striatal interneurons are similar to prior studies in the striatum of HD patients. Also, the pathological differences observed between rHD1 and rHD7 suggest two distinct pathological patterns of HD that resemble juvenile and adult forms of HD, respectively. Finally, it can be speculated that CR and PV proteins have neuroprotective functions via the regulation of intracellular calcium concentrations and maintenance of calcium homeostasis.

## **Future Directions**

### *Nissl Staining to Quantify the Total Number of Striatal Neurons*

We would like to perform Nissl staining on rHD1, rHD7, and rWT1 to estimate the total number of striatal cells in these NHPs via stereology. Using this information, we would be able to calculate the percent of total cells that are CR+, PV+, and ChAT+ cells in the striatum. There are data from HD patients and age-matched controls that assess the percentage of the different types of interneurons in the striatum, and this method would allow us to compare our model to human patients in this regard.

### *Quantify Genetic Expression Levels of Striatal Neurons via Quantitative PCR*

HD patients show dysregulation of gene expression, especially in the striatum (Hodges et al., 2006). To further validate our HD-NHP model, we will conduct quantitative real-time PCR (qPCR) and test for various genes known to be dysregulated. This would also allow us to determine if CR, PV, and ChAT expression are upregulated in HD. Many of the genes we have picked regulate markers that function as part of the basal ganglia-thalamocortical circuitry, a system known to be affected in HD. We will design primers based on the human sequence of the genes and test the efficacy of the primer against mixed brain sample from a WT-NHP. Once confirmed, we will run the primers against striatal tissue samples from HD- and WT-NHPs. We will compare the expression levels between our HD-NHPs, and compare our HD-NHPs with WT-NHPs. We will also compare the change in expression levels of our HD-NHPs with levels seen in HD patients.

## Figures

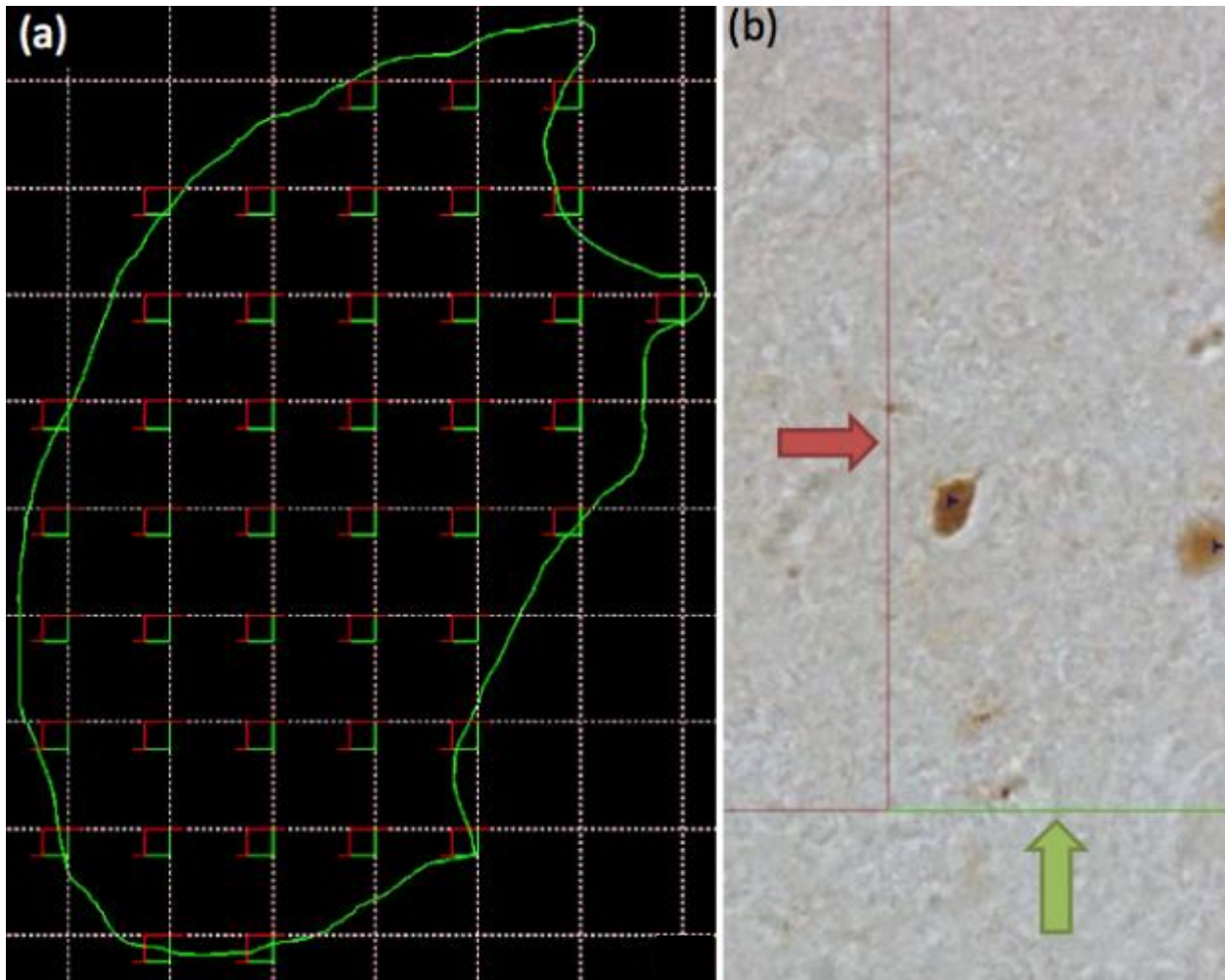


*Figure 1. Stereology*

(a) Optical fractionator grid (white lines) and counting probes (red and green squares) at 2.5x.

The ROI is traced in green. (b) The stereology probe under 40x oil-immersion. Depicted are the acceptance (green) and rejection (red) lines.

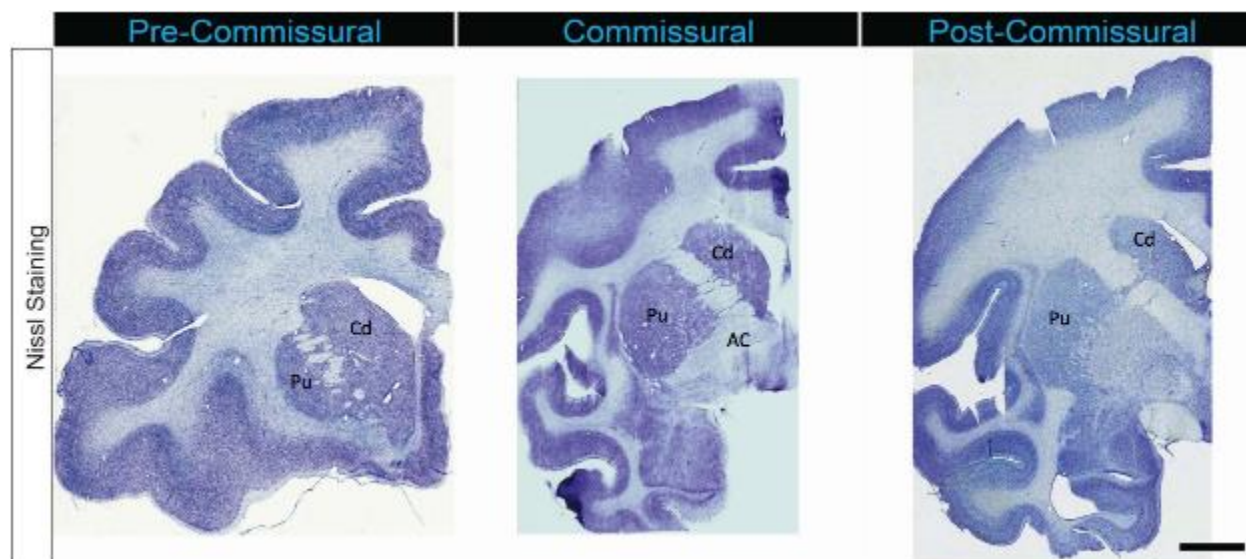


*Figure 2. Pre- and Post-Commissural Regions*

Scanned images of Nissl-stained coronal brain sections (50 $\mu$ m) depicting the striatal ROIs – the caudate nucleus (Cd) and putamen (Pu). The middle micrograph shows the anterior commissure (AC), which is used as the landmark that distinguishes the head (in front of the AC) from the body (behind the AC) of the caudate nucleus, and the pre- from the post-commissural regions of the putamen. The scale bar represents 5mm.

		<b>CR+</b>		<b>PV+</b>		<b>ChAT+</b>	
		<i>Number of sections</i>	<i>Interval Number</i>	<i>Number of sections</i>	<i>Interval Number</i>	<i>Number of sections</i>	<i>Interval Number</i>
<b>rWT1</b>	Pre-Commissural	8	1/15	8	1/15	6	1/24
	Post-Commissural	16	1/15	16	1/15	11	1/24
<b>rHD7</b>	Pre-Commissural	6	1/24	5	1/24	15	1/12
	Post-Commissural	8	1/24	7	1/24	19	1/12
<b>rHD1</b>	Pre-Commissural	5	1/24	4	1/24	9	1/12
	Post-Commissural	7	1/24	5	1/24	13	1/12

*Table 1. Number of Sections and Serial Section Interval Number*

The number of sections that were stained with each immunomarker and the serial section interval number for each immunomarker and NHP.

<b>Target</b>	<b>Grid/Probe</b>	<b>Caudate Nucleus</b>	<b>Putamen</b>
CR	Grid	700 $\mu\text{m}$ x 700 $\mu\text{m}$	1200 $\mu\text{m}$ x 1200 $\mu\text{m}$
	Probe	300 $\mu\text{m}$ x 300 $\mu\text{m}$	300 $\mu\text{m}$ x 300 $\mu\text{m}$
PV	Grid	700 $\mu\text{m}$ x 700 $\mu\text{m}$	800 $\mu\text{m}$ x 800 $\mu\text{m}$
	Probe	300 $\mu\text{m}$ x 300 $\mu\text{m}$	400 $\mu\text{m}$ x 400 $\mu\text{m}$
ChAT	Grid	1400 $\mu\text{m}$ x 1400 $\mu\text{m}$	1400 $\mu\text{m}$ x 1400 $\mu\text{m}$
	Probe	600 $\mu\text{m}$ x 600 $\mu\text{m}$	600 $\mu\text{m}$ x 600 $\mu\text{m}$

*Table 2. Optical Fractionator Grid and Counting Probe Size*

The optical fractionator grid and counting probe size. The dimensions were chosen to maximize efficiency and minimize the CE.

	<b>Caudate Nucleus</b>						<b>Putamen</b>					
	<i>Head</i>			<i>Body</i>			<i>Pre</i>			<i>Post</i>		
	Total Cell Count	CE	Percent Difference from rWT1	Total Cell Count	CE	Percent Difference from rWT1	Total Cell Count	CE	Percent Difference from rWT1	Total Cell Count	CE	Percent Difference from rWT1
<b>CR+</b>												
rWT1	4.01x10 <sup>5</sup>	0.02	-	2.83x10 <sup>5</sup>	0.02	-	2.25x10 <sup>5</sup>	0.04	-	4.43x10 <sup>5</sup>	0.03	-
rHD7	4.43x10 <sup>5</sup>	0.02	+10.4% ↑	2.21x10 <sup>5</sup>	0.03	-22.1% ↓	2.45x10 <sup>5</sup>	0.05	+8.6% ↑	3.20x10 <sup>5</sup>	0.04	-27.8% ↓
rHD1	3.37x10 <sup>5</sup>	0.03	-16.1% ↓	1.63x10 <sup>5</sup>	0.04	-42.4% ↓	2.26x10 <sup>5</sup>	0.05	+0.2% ↑	2.46x10 <sup>5</sup>	0.04	-44.5% ↓
<b>PV+</b>												
rWT1	1.24x10 <sup>5</sup>	0.04	-	1.72x10 <sup>5</sup>	0.03	-	1.24x10 <sup>5</sup>	0.04	-	4.74x10 <sup>5</sup>	0.03	-
rHD7	6.79x10 <sup>4</sup>	0.06	-46.6% ↓	3.53x10 <sup>4</sup>	0.07	-79.5% ↓	8.37x10 <sup>4</sup>	0.05	-32.4% ↓	1.73x10 <sup>5</sup>	0.04	-63.6% ↓
rHD1	5.55x10 <sup>4</sup>	0.06	-56.4% ↓	4.27x10 <sup>4</sup>	0.06	-75.2% ↓	1.15x10 <sup>5</sup>	0.05	-7.6% ↓	2.90x10 <sup>5</sup>	0.03	-38.9% ↓
<b>ChAT+</b>												
rWT1	8.52x10 <sup>4</sup>	0.05	-	8.78x10 <sup>4</sup>	0.06	-	1.10x10 <sup>5</sup>	0.05	-	2.60x10 <sup>5</sup>	0.03	-
rHD7	9.49x10 <sup>4</sup>	0.04	+11.4% ↑	3.84x10 <sup>4</sup>	0.06	-56.3% ↓	5.75x10 <sup>4</sup>	0.05	-47.8% ↓	3.01x10 <sup>4</sup>	0.06	-88.4% ↓
rHD1	1.08x10 <sup>5</sup>	0.03	+27.1% ↑	7.73x10 <sup>4</sup>	0.04	-12.0% ↓	8.31x10 <sup>4</sup>	0.04	-24.5% ↓	1.32x10 <sup>5</sup>	0.03	-49.4% ↓

*Table 3. Interneuron Counts and Percent Difference*

Estimated total stereological counts for each interneuron and percent difference from rWT1 (control). Negative percentages indicate a lower number relative to the control, while a positive percentage indicates a higher number relative to the control. “Pre” and “Post” refer to the pre-commissural and post-commissural region of the striatum, respectively.

	<b>Caudate Nucleus</b>						<b>Putamen</b>					
	<i>Head</i>			<i>Body</i>			<i>Pre</i>			<i>Post</i>		
	Total Volume (mm <sup>3</sup> )	CE	Percent Difference from rWT1	Total Volume (mm <sup>3</sup> )	CE	Percent Difference from rWT1	Total Volume (mm <sup>3</sup> )	CE	Percent Difference from rWT1	Total Volume (mm <sup>3</sup> )	CE	Percent Difference from rWT1
<b>CR+</b>												
rWT1	155.9	0.02	-	139.9	0.01	-	178.8	0.015	-	487.2	0.007	-
rHD7	207.5	0.02	+33.2% ↑	119.4	0.03	-14.7% ↓	201.0	0.017	+12.4% ↑	386.3	0.016	-20.7% ↓
rHD1	62.3	0.02	-60.0% ↓	50.88	0.03	-63.6% ↓	83.9	0.026	-53.1% ↓	130.9	0.016	-73.1% ↓
<b>PV+</b>												
rWT1	182.9	0.01	-	145.9	0.01	-	205.3	0.01	-	489.4	0.01	-
rHD7	190.7	0.02	+4.3% ↑	105.8	0.02	-27.5% ↓	210.2	0.01	+2.4% ↑	319.1	0.01	-34.8% ↓
rHD1	87.9	0.03	-51.9% ↓	56.1	0.03	-61.6% ↓	88.9	0.03	-56.7% ↓	114.0	0.03	-76.7% ↓
<b>ChAT+</b>												
rWT1	215.2	0.01	-	157.6	0.02	-	268.6	0.02	-	490.0	0.01	-
rHD7	289.5	0.01	+34.5% ↑	95.6	0.01	-39.3%	319.1	0.01	+18.8% ↑	402.8	0.01	-17.8% ↓
rHD1	106.4	0.01	-50.6% ↓	60.6	0.02	-61.6%	104.5	0.01	-61.1% ↓	138.4	0.01	-71.7% ↓

*Table 4. Striatal Volume and Percent Difference*

Estimated striatal volume determined for each serial section and percent difference from rWT1 (control). Negative percentages indicate a lower number relative to the control, while a positive percentage indicates a higher number relative to the control. “Pre” and “Post” refer to the pre-commissural and post-commissural region of the striatum, respectively.

	<b>Caudate Nucleus</b>				<b>Putamen</b>			
	<i>Head</i>		<i>Body</i>		<i>Pre</i>		<i>Post</i>	
	Density (n/mm <sup>3</sup> )	Percent Difference from rWT1	Density (n/mm <sup>3</sup> )	Percent Difference from rWT1	Density (n/mm <sup>3</sup> )	Percent Difference from rWT1	Density (n/mm <sup>3</sup> )	Percent Difference from rWT1
CR+								
rWT1	2.58x10 <sup>3</sup>	-	2.02x10 <sup>3</sup>	-	1.26 x10 <sup>3</sup>	-	9.10 x10 <sup>2</sup>	-
rHD7	2.14x10 <sup>3</sup>	-17.1% ↓	1.85x10 <sup>3</sup>	-8.7% ↓	1.22 x10 <sup>3</sup>	-3.4% ↓	8.29 x10 <sup>2</sup>	-8.9% ↓
rHD1	5.40x10 <sup>3</sup>	+109.9% ↑	3.2x10 <sup>3</sup>	+58.4% ↑	2.70 x10 <sup>3</sup>	+113.6% ↑	1.88 x10 <sup>3</sup>	+106.6% ↑
PV+								
rWT1	6.95x10 <sup>2</sup>	-	1.18x10 <sup>3</sup>	-	6.03x10 <sup>2</sup>	-	9.69x10 <sup>2</sup>	-
rHD7	3.56x10 <sup>2</sup>	-48.8% ↓	3.33x10 <sup>2</sup>	-71.8% ↓	3.98x10 <sup>2</sup>	-34.0% ↓	5.41x10 <sup>2</sup>	-44.2% ↓
rHD1	6.3x10 <sup>2</sup>	-9.3% ↓	7.61x10 <sup>2</sup>	-35.6% ↓	1.29x10 <sup>3</sup>	+113.4% ↑	2.54x10 <sup>3</sup>	+162.0% ↑
ChAT+								
rWT1	3.95x10 <sup>2</sup>	-	5.57x10 <sup>2</sup>	-	4.10x10 <sup>2</sup>	-	5.31x10 <sup>2</sup>	-
rHD7	3.28x10 <sup>2</sup>	-17.2% ↓	4.01x10 <sup>2</sup>	-28.0% ↓	1.80x10 <sup>2</sup>	-56.1% ↓	7.48x10 <sup>1</sup>	-85.9% ↓
rHD1	1.02x10 <sup>3</sup>	+157.2% ↑	1.28x10 <sup>3</sup>	+129.0% ↑	7.95x10 <sup>2</sup>	+94.0% ↑	9.52x10 <sup>2</sup>	+79.3% ↑

*Table 5. Interneuron Density and Percent Difference*

Density of each interneuron type and percent difference from rWT1 (control). Negative percentages indicate a lower number relative to the control, while a positive percentage indicates a higher number relative to the control. n = estimated number of neurons. “Pre” and “Post” refer to the pre-commissural and post-commissural region of the striatum, respectively.

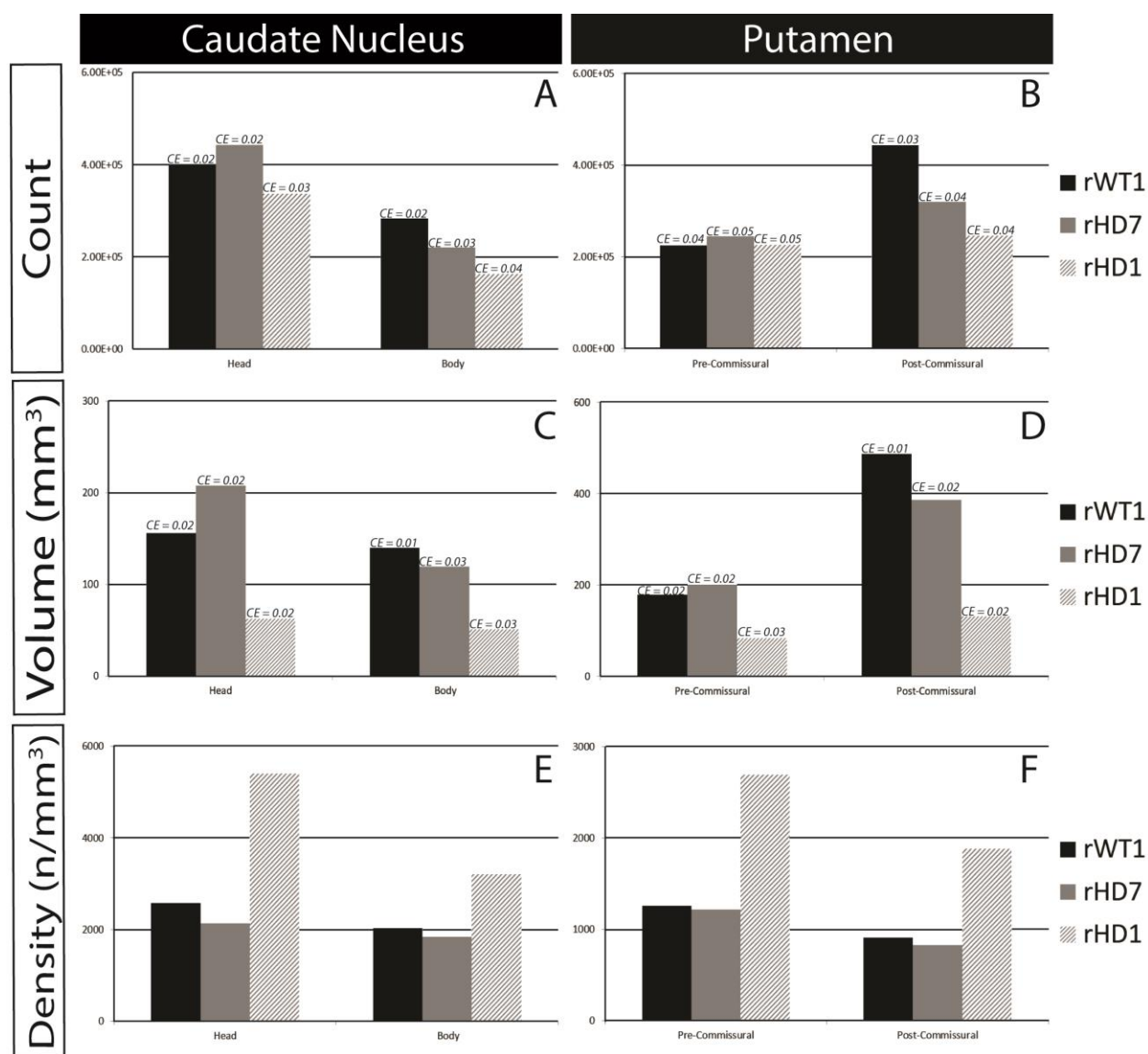


*Figure 3. Stereological Counts of CR+ Neurons*

Estimated total number of CR+ interneurons in the (A) caudate nucleus and (B) putamen in transgenic HD and control NHPs. Estimated total volume of the (C) caudate nucleus and (D) putamen were used to determine the (E-F) density of CR+ interneurons in the striatum. The CE was at or below 0.05 for all measurements above.

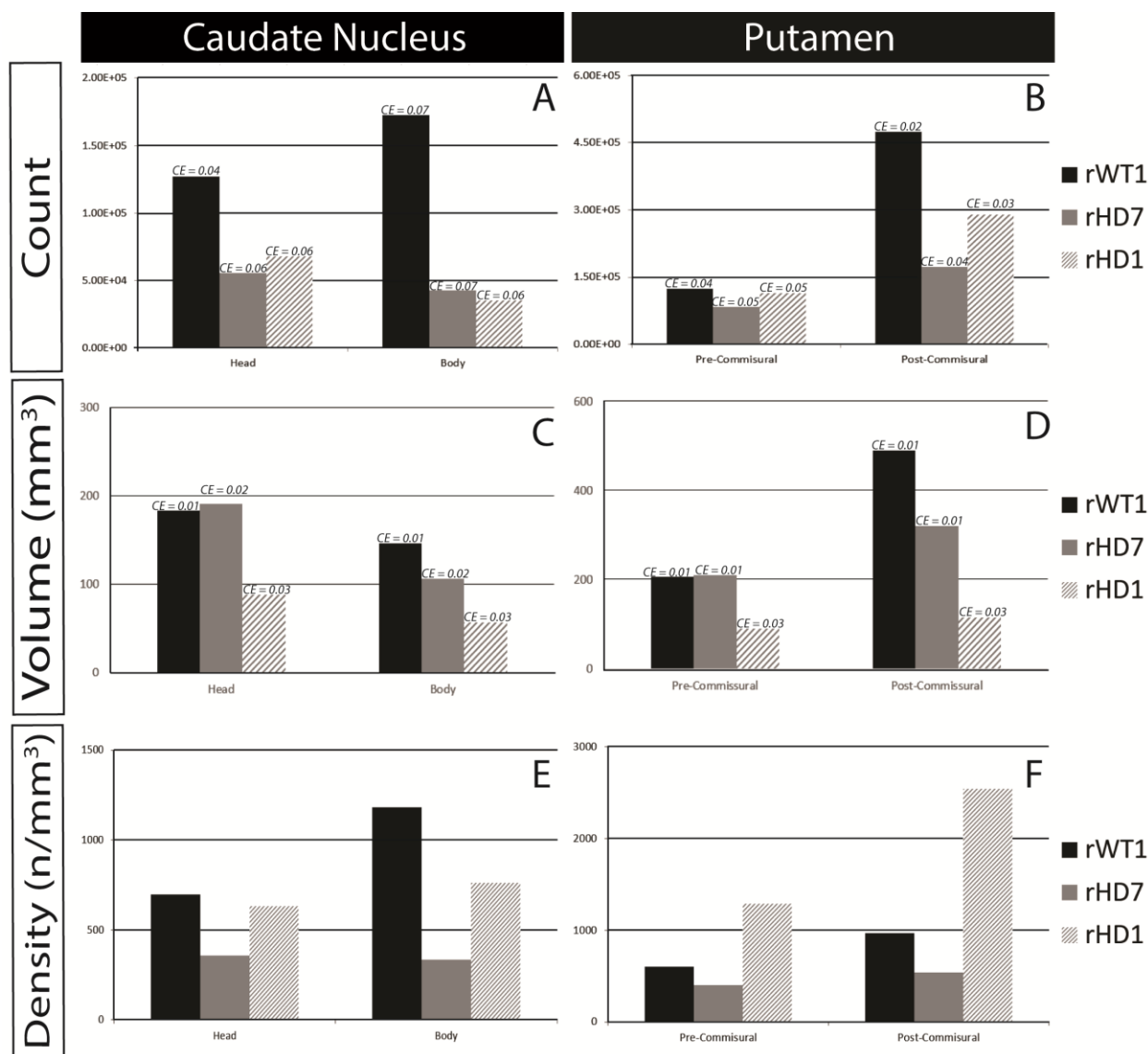


Figure 4. Stereological Counts of PV+ Neurons

Estimated total number of PV+ interneurons in the (A) caudate nucleus and (B) putamen in transgenic HD and control NHPs. Estimated total volume of the (C) caudate nucleus and (D) putamen were used to determine the (E-F) density of PV+ interneurons in the striatum. The CE was at or below 0.07 for all measurements above.

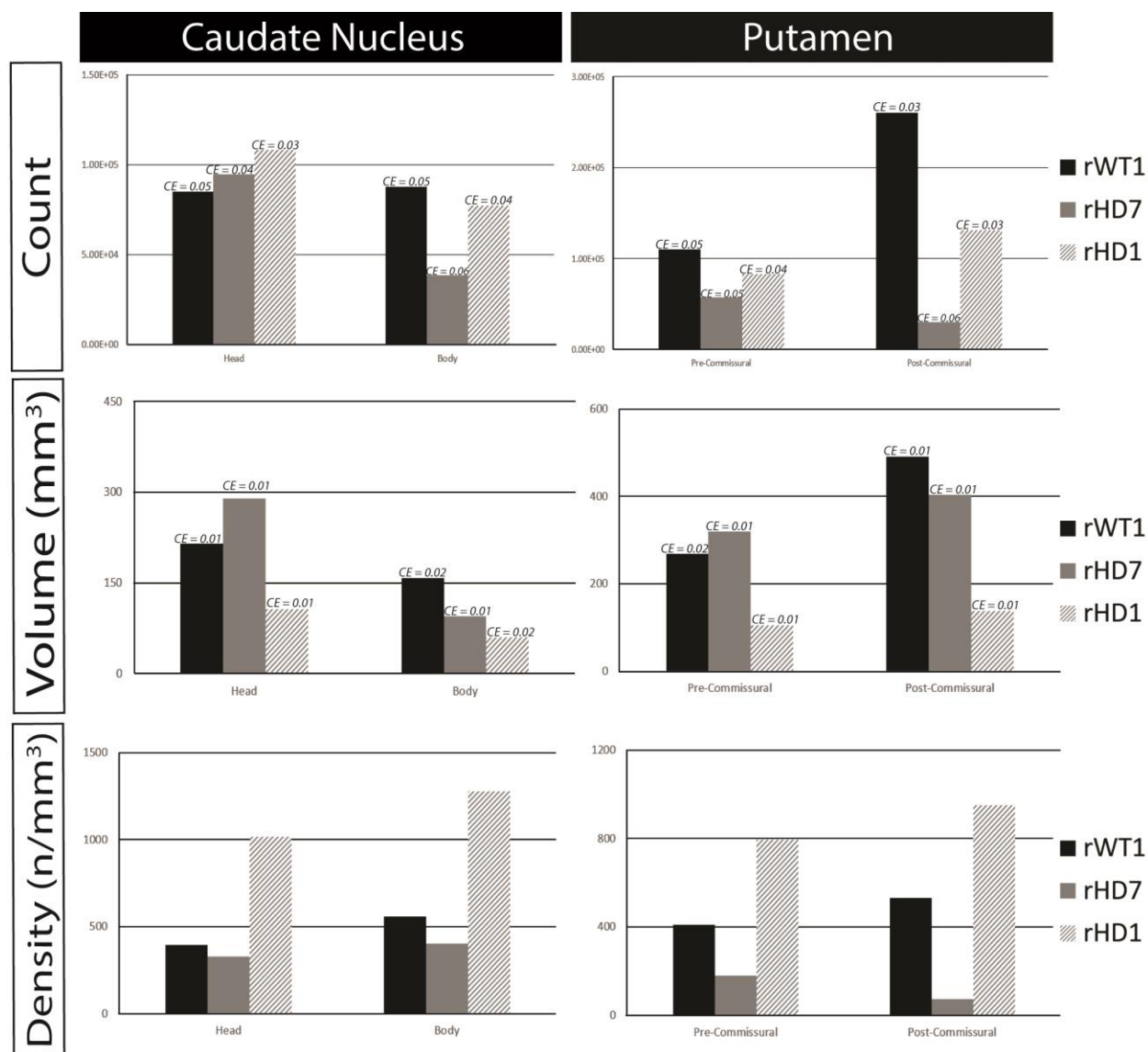
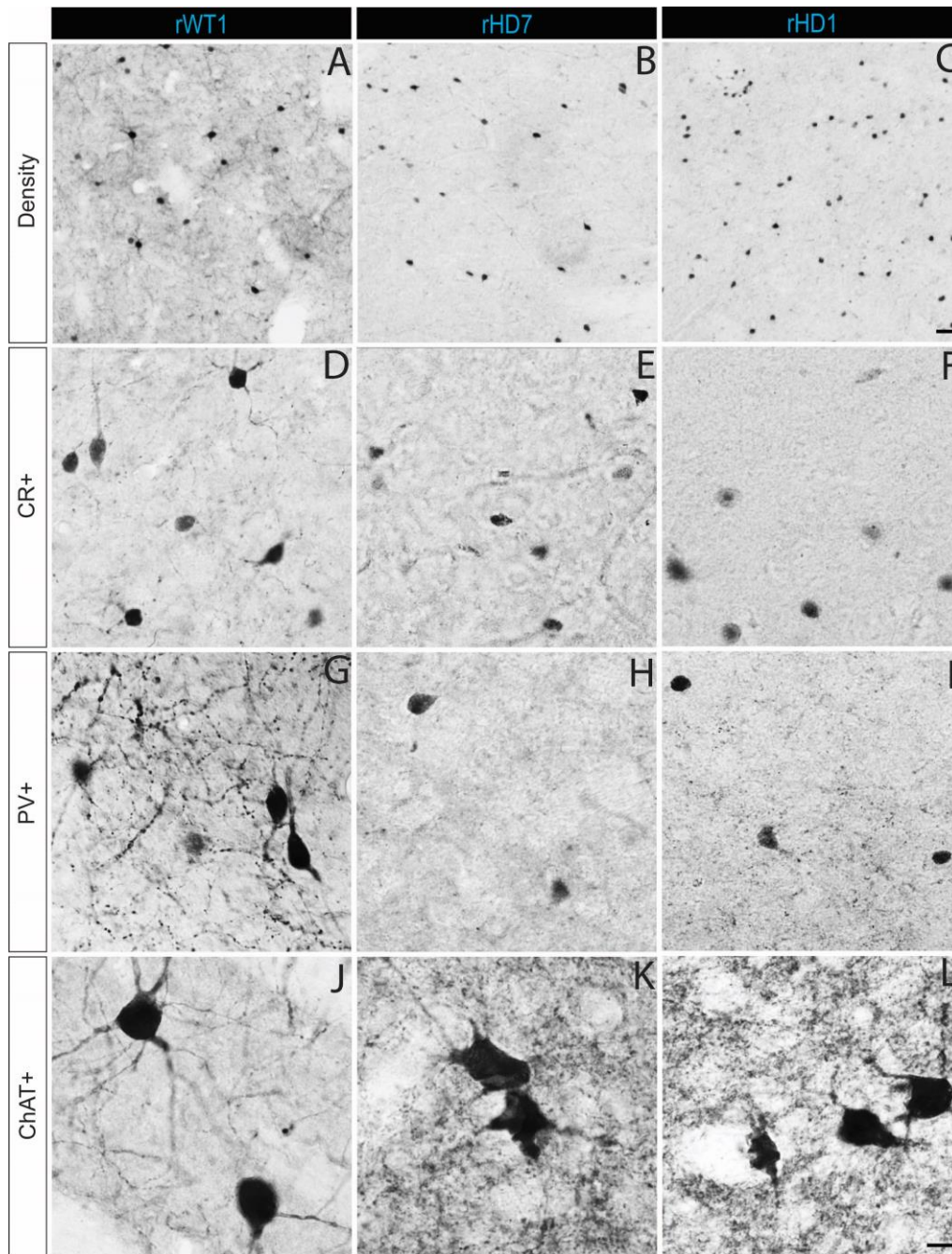


Figure 5. Stereological Counts of ChAT+ Neurons

Total number of ChAT+ interneurons in the (A) caudate nucleus and (B) putamen in transgenic HD and control NHPs. Total volume of the (C) caudate nucleus and (D) putamen were used to determine the (E-F) density of ChAT+ interneurons in the striatum. The CE was at or below 0.06 for all measurements above.



*Figure 6. Light Micrographs of Immunostained Striatal Interneurons*

(A-C) Light microscope images depicting the differences in density of CR<sup>+</sup> cells in the caudate head between the transgenic HD- and WT-NHPs. The scale bar in C represents 20  $\mu$ m. (D-L) Light microscope images depicting the of CR<sup>+</sup>, PV<sup>+</sup>, and ChAT<sup>+</sup> neurons in each NHP. The scale bar in L represents 10  $\mu$ m.

## References

- Altunkaynak BZ, Onger ME, Altunkaynak ME, Ayranci E, Canan S (2012) A Brief Introduction to Stereology and Sampling Strategies: Basic Concepts of Stereology. *Neuroquantology* 10:31-43.
- Andre VM, Fisher YE, Levine MS (2011) Altered Balance of Activity in the Striatal Direct and Indirect Pathways in Mouse Models of Huntington's Disease. *Front Syst Neurosci* 5:46.
- Burns LH, Pakzaban P, Deacon TW, Brownell AL, Tatter SB, Jenkins BG, Isacson O (1995) Selective putaminal excitotoxic lesions in non-human primates model the movement disorder of Huntington disease. *Neuroscience* 64:1007-1017.
- Calabresi P, Picconi B, Tozzi A, Ghiglieri V, Di Filippo M (2014) Direct and indirect pathways of basal ganglia: a critical reappraisal. *Nat Neurosci* 17:1022-1030.
- Carter RL, Chen Y, Kunkanjanawan T, Xu Y, Moran SP, Putkhao K, Yang J, Huang AH, Parnpai R, Chan AW (2014) Reversal of cellular phenotypes in neural cells derived from Huntington's disease monkey-induced pluripotent stem cells. *Stem Cell Reports* 3:585-593.
- Centonze D, Bernardi G, Koch G (2007) Mechanisms of disease: basic-research-driven investigations in humans--the case of hyperkinetic disorders. *Nat Clin Pract Neurol* 3:572-580.
- Cepeda C, Wu N, Andre VM, Cummings DM, Levine MS (2007) The corticostriatal pathway in Huntington's disease. *Prog Neurobiol* 81:253-271.
- Chan AW et al. (2014) A two years longitudinal study of a transgenic Huntington disease monkey. *BMC Neurosci* 15:36.

- Chan AWS, Jiang J, Chen YJ, Li CX, Prucha MS, Hu YJ, Chi T, Moran S, Rahim T, Li SH, Li XJ, Zola SM, Testa CM, Mao H, Villalba R, Smith Y, Zhang XD, Bachevalier J (2015) Progressive Cognitive Deficit, Motor Impairment and Striatal Pathology in a Transgenic Huntington Disease Monkey Model from Infancy to Adulthood. *Plos One* 10.
- Cicchetti F, Parent A (1996) Striatal interneurons in Huntington's disease: selective increase in the density of calretinin-immunoreactive medium-sized neurons. *Mov Disord* 11:619-626.
- Cicchetti F, Gould PV, Parent A (1996) Sparing of striatal neurons coexpressing calretinin and substance P (NK1) receptor in Huntington's disease. *Brain Res* 730:232-237.
- Cicchetti F, Beach TG, Parent A (1998) Chemical phenotype of calretinin interneurons in the human striatum. *Synapse* 30:284-297.
- Cicchetti F, Prensa L, Wu Y, Parent A (2000) Chemical anatomy of striatal interneurons in normal individuals and in patients with Huntington's disease. *Brain Res Brain Res Rev* 34:80-101.
- Cui G, Jun SB, Jin X, Pham MD, Vogel SS, Lovinger DM, Costa RM (2013) Concurrent activation of striatal direct and indirect pathways during action initiation. *Nature* 494:238-242.
- Davies SW, Turmaine M, Cozens BA, DiFiglia M, Sharp AH, Ross CA, Scherzinger E, Wanker EE, Mangiarini L, Bates GP (1997) Formation of neuronal intranuclear inclusions underlies the neurological dysfunction in mice transgenic for the HD mutation. *Cell* 90:537-548.

- DiFiglia M, Sapp E, Chase KO, Davies SW, Bates GP, Vonsattel JP, Aronin N (1997) Aggregation of huntingtin in neuronal intranuclear inclusions and dystrophic neurites in brain. *Science* 277:1990-1993.
- Feigin A, Kiebertz K, Bordwell K, Como P, Steinberg K, Sotack J, Zimmerman C, Hickey C, Orme C, Shoulson I (1995) Functional decline in Huntington's disease. *Mov Disord* 10:211-214.
- Ferrante RJ, Kowall NW, Cipolloni PB, Storey E, Beal MF (1993) Excitotoxin lesions in primates as a model for Huntington's disease: histopathologic and neurochemical characterization. *Exp Neurol* 119:46-71.
- Fong CY, Gauthaman K, Bongso A (2010) Teratomas from pluripotent stem cells: A clinical hurdle. *J Cell Biochem* 111:769-781.
- Gil JM, Rego AC (2008) Mechanisms of neurodegeneration in Huntington's disease. *Eur J Neurosci* 27:2803-2820.
- Glaser EM, Wilson PD (1998) The coefficient of error of optical fractionator population size estimates: a computer simulation comparing three estimators. *J Microsc* 192:163-171.
- Halliday GM, McRitchie DA, Macdonald V, Double KL, Trent RJ, McCusker E (1998) Regional specificity of brain atrophy in Huntington's disease. *Exp Neurol* 154:663-672.
- Hansson O, Guatteo E, Mercuri NB, Bernardi G, Li XJ, Castilho RF, Brundin P (2001) Resistance to NMDA toxicity correlates with appearance of nuclear inclusions, behavioural deficits and changes in calcium homeostasis in mice transgenic for exon 1 of the huntington gene. *Eur J Neurosci* 14:1492-1504.
- Herculano-Houzel S (2009) The human brain in numbers: a linearly scaled-up primate brain. *Front Hum Neurosci* 3:31.

- Hodges A et al. (2006) Regional and cellular gene expression changes in human Huntington's disease brain. *Hum Mol Genet* 15:965-977.
- Illarioshkin SN, Igarashi S, Onodera O, Markova ED, Nikolskaya NN, Tanaka H, Chabrashwili TZ, Insarova NG, Endo K, Ivanova-Smolenskaya IA, et al. (1994) Trinucleotide repeat length and rate of progression of Huntington's disease. *Ann Neurol* 36:630-635.
- Juopperi TA, Kim WR, Chiang CH, Yu H, Margolis RL, Ross CA, Ming GL, Song H (2012) Astrocytes generated from patient induced pluripotent stem cells recapitulate features of Huntington's disease patient cells. *Mol Brain* 5:17.
- Kendall AL, David F, Rayment G, Torres EM, Annett LE, Dunnett SB (2000) The influence of excitotoxic basal ganglia lesions on motor performance in the common marmoset. *Brain* 123 ( Pt 7):1442-1458.
- Luthi-Carter R, Strand A, Peters NL, Solano SM, Hollingsworth ZR, Menon AS, Frey AS, Spektor BS, Penney EB, Schilling G, Ross CA, Borchelt DR, Tapscott SJ, Young AB, Cha JH, Olson JM (2000) Decreased expression of striatal signaling genes in a mouse model of Huntington's disease. *Hum Mol Genet* 9:1259-1271.
- Massouh M, Wallman MJ, Pourcher E, Parent A (2008) The fate of the large striatal interneurons expressing calretinin in Huntington's disease. *Neurosci Res* 62:216-224.
- Menalled LB, Chesselet MF (2002) Mouse models of Huntington's disease. *Trends Pharmacol Sci* 23:32-39.
- Morton AJ, Howland DS (2013) Large genetic animal models of Huntington's Disease. *J Huntingtons Dis* 2:3-19.

- Morton AJ, Lagan MA, Skepper JN, Dunnett SB (2000) Progressive formation of inclusions in the striatum and hippocampus of mice transgenic for the human Huntington's disease mutation. *J Neurocytol* 29:679-702.
- Nasir J, Floresco SB, O'Kusky JR, Diewert VM, Richman JM, Zeisler J, Borowski A, Marth JD, Phillips AG, Hayden MR (1995) Targeted disruption of the Huntington's disease gene results in embryonic lethality and behavioral and morphological changes in heterozygotes. *Cell* 81:811-823.
- O'Donovan MC (1993) A novel gene containing a trinucleotide repeat that is expanded and unstable on Huntington's disease chromosomes. The Huntington's Disease Collaborative Research Group. *Cell* 72:971-983.
- Ordway JM, Tallaksen-Greene S, Gutekunst CA, Bernstein EM, Cearley JA, Wiener HW, Dure LS, Lindsey R, Hersch SM, Jope RS, Albin RL, Detloff PJ (1997) Ectopically expressed CAG repeats cause intranuclear inclusions and a progressive late onset neurological phenotype in the mouse. *Cell* 91:753-763.
- Parent A, Cicchetti F, Beach TG (1995) Calretinin-immunoreactive neurons in the human striatum. *Brain Res* 674:347-351.
- Penney JB, Jr., Vonsattel JP, MacDonald ME, Gusella JF, Myers RH (1997) CAG repeat number governs the development rate of pathology in Huntington's disease. *Ann Neurol* 41:689-692.
- Petryszyn S, Beaulieu JM, Parent A, Parent M (2014) Distribution and morphological characteristics of striatal interneurons expressing calretinin in mice: a comparison with human and nonhuman primates. *J Chem Neuroanat* 59-60:51-61.

- Pringsheim T, Wiltshire K, Day L, Dykeman J, Steeves T, Jette N (2012) The incidence and prevalence of Huntington's disease: a systematic review and meta-analysis. *Mov Disord* 27:1083-1091.
- Putkhao K, Chan AW, Agca Y, Parnpai R (2013) Cryopreservation of transgenic Huntington's disease rhesus macaque sperm-A Case Report. *Cloning Transgenes* 2.
- Quarrell O, O'Donovan KL, Bandmann O, Strong M (2012) The Prevalence of Juvenile Huntington's Disease: A Review of the Literature and Meta-Analysis. *PLoS Curr* 4:e4f8606b8742ef8603.
- Quarrell OW, Nance MA, Nopoulos P, Paulsen JS, Smith JA, Squitieri F (2013) Managing juvenile Huntington's disease. *Neurodegener Dis Manag* 3.
- Raper J, Bosinger S, Johnson Z, Tharp G, Moran SP, Chan AW (2016) Increased irritability, anxiety, and immune reactivity in transgenic Huntington's disease monkeys. *Brain Behav Immun*.
- Reiner A, Albin RL, Anderson KD, D'Amato CJ, Penney JB, Young AB (1988) Differential loss of striatal projection neurons in Huntington disease. *Proc Natl Acad Sci U S A* 85:5733-5737.
- Ross CA, Tabrizi SJ (2011) Huntington's disease: from molecular pathogenesis to clinical treatment. *Lancet Neurol* 10:83-98.
- Rub U, Seidel K, Heinsen H, Vonsattel JP, den Dunnen WF, Korf HW (2016) Huntington's disease (HD): the neuropathology of a multisystem neurodegenerative disorder of the human brain. *Brain Pathol* 26:726-740.
- Rubinsztein DC (2002) Lessons from animal models of Huntington's disease. *Trends Genet* 18:202-209.

- Rubinsztein DC et al. (1996) Phenotypic characterization of individuals with 30-40 CAG repeats in the Huntington disease (HD) gene reveals HD cases with 36 repeats and apparently normal elderly individuals with 36-39 repeats. *Am J Hum Genet* 59:16-22.
- Schulte J, Littleton JT (2011) The biological function of the Huntingtin protein and its relevance to Huntington's Disease pathology. *Curr Trends Neurol* 5:65-78.
- Smith Y, Bevan MD, Shink E, Bolam JP (1998) Microcircuitry of the direct and indirect pathways of the basal ganglia. *Neuroscience* 86:353-387.
- Storey E, Cipolloni PB, Ferrante RJ, Kowall NW, Beal MF (1994) Movement disorder following excitotoxin lesions in primates. *Neuroreport* 5:1259-1261.
- Treuting PM, Dintzis SM, Frevert CW, Liggitt HD, Montine KS (2012) Comparative anatomy and histology : a mouse and human atlas, 1st Edition. Amsterdam ; Boston: Elsevier/Academic Press.
- Vonsattel JP, Myers RH, Stevens TJ, Ferrante RJ, Bird ED, Richardson EP, Jr. (1985) Neuropathological classification of Huntington's disease. *J Neuropathol Exp Neurol* 44:559-577.
- Walker FO (2007) Huntington's disease. *Lancet* 369:218-228.
- West MJ (2012) Introduction to stereology. *Cold Spring Harb Protoc* 2012.
- Wu Y, Parent A (2000) Striatal interneurons expressing calretinin, parvalbumin or NADPH-diaphorase: a comparative study in the rat, monkey and human. *Brain Res* 863:182-191.
- Yang SH, Cheng PH, Banta H, Piotrowska-Nitsche K, Yang JJ, Cheng EC, Snyder B, Larkin K, Liu J, Orkin J, Fang ZH, Smith Y, Bachevalier J, Zola SM, Li SH, Li XJ, Chan AW (2008) Towards a transgenic model of Huntington's disease in a non-human primate. *Nature* 453:921-924.

Zuccato C, Ciammola A, Rigamonti D, Leavitt BR, Goffredo D, Conti L, MacDonald ME,

Friedlander RM, Silani V, Hayden MR, Timmusk T, Sipione S, Cattaneo E (2001) Loss of huntingtin-mediated BDNF gene transcription in Huntington's disease. *Science* 293:493-498.

Zucker B, Luthi-Carter R, Kama JA, Dunah AW, Stern EA, Fox JH, Standaert DG, Young AB,

Augood SJ (2005) Transcriptional dysregulation in striatal projection- and interneurons in a mouse model of Huntington's disease: neuronal selectivity and potential neuroprotective role of HAP1. *Hum Mol Genet* 14:179-189.